

Computation of wind-wave spectra in coastal waters with SWAN on unstructured grids

M. Zijlema*

Environmental Fluid Mechanics Section, Faculty of Civil Engineering and Geosciences, Delft University of Technology, P.O. Box 5048, 2600 GA Delft, The Netherlands

ARTICLE INFO

Article history:

Received 19 August 2008
 Received in revised form 7 October 2009
 Accepted 19 October 2009
 Available online 14 November 2009

Keywords:

Wind-wave spectra
 SWAN
 Unstructured grid
 Finite difference
 Fully implicit

ABSTRACT

An unstructured-grid procedure for SWAN is presented. It is a vertex-based, fully implicit, finite difference method which can accommodate unstructured meshes with a high variability in geographic resolution suitable for representing complicated bottom topography in shallow areas and irregular shoreline. The numerical solution is found by means of a point-to-point multi-directional Gauss–Seidel iteration method requiring a number of sweeps through the grid. The approach is stable for any time step while permitting local mesh refinements in areas of interest. A number of applications are shown to verify the correctness and numerical accuracy of the unstructured version of SWAN.

© 2009 Elsevier B.V. All rights reserved.

1. Introduction

For many years, numerical modelling of wind waves has been successfully addressed by means of third-generation spectral wave models that calculate spectra of random short-crested, wind-generated waves and swell in both offshore and coastal regions. The kinematic behaviour of the waves is described with the linear theory for surface gravity waves whereas the wave dynamics are associated with the processes of generation, dissipation and nonlinear wave–wave interactions (Holthuijsen, 2007). Examples of well-established third-generation spectral wave models are WAM (WAMDI Group, 1988), WAVEWATCH III (Tolman, 1991) and SWAN (Booij et al., 1999).

While spectral wave models mainly focus on large-scale wind-wave and wave–wave interactions, wave features on small scale associated with irregular bathymetry, e.g. surf breaking, triad and wave–current interactions, are critical to understanding wave dynamics and assessing impacts of engineering activities. This is especially important in coastal areas. Therefore, there is a strong need for accurate spectral wave simulations allowing to better understand and analyse the interactions between wind, waves and currents in e.g., estuaries, fjords, tidal inlets, lakes, marshes and channels. In particular, a highly-resolved model is desired for modelling such a system.

Since, the characteristic spatial scales of the wind waves propagating from deep to shallow waters are very diverse, a flexible grid would be required to increase effectively the resolution near shore without incurring overhead associated with grid adaptation at some distance offshore. Traditionally, this can be achieved by employing a

nesting technique, where finer grids are nested within coarser grids. Although, this practise is very common for spectral models, it does not always result in optimality for a number of reasons. First, an interpolation procedure must be applied from coarse to fine grids. Although, interpolation is not conceptually difficult, it is a disadvantage because it is costly to perform. Second, nested meshes introduce additional boundaries where problems often occur due to mismatches in numerics and/or physics. Different accuracy properties or abruptly local changes in physics can make it difficult to apply the solution from one grid model as a boundary condition in another grid. Finally, in one-way nesting, there is no feedback between the fine and coarse grids, while in two-way nesting, the solution is fully coupled at the coarse–fine interface requiring an iterative run process.

This coarse–fine grid nesting approach is an example of a classic trade-off that is experienced in coastal environmental problems. Better physics require better resolution, but that resolution can be costly. Hence, one must choose a level of resolution that captures the important physics without sacrificing computational efficiency.

The use of unstructured grids offers a good alternative to nested models not only because of the ease of local grid refinement, either fixed or adaptive, but also the high flexibility to generate grids along coastline and around islands. Unstructured meshes with variable resolution provide the capability to simultaneously capture scales ranging many orders of magnitude, e.g. from hundreds of kilometers to tens of meters. The variable mesh is especially useful in coastal regions where the water depth varies greatly, thus giving the highest resolution where it is most needed. Moreover, this can be automated to a large extent. For instance, there exist techniques for triangulation of arbitrary geometries (see e.g. Shewchuk, 1996; Bilgili and Smith, 2003). An unstructured mesh also allows for a very large domain with locally refined grid. As the response in deep water is generally less

* Tel.: +31 15 278 3255; fax: +31 15 278 4842.

E-mail address: m.zijlema@tudelft.nl.

involved than in the surf zone, large domains with open boundaries in the deep ocean greatly simplify the task of boundary condition specification. Although, the CPU cost per grid point is often relative higher than in cases with structured grids, this effect is probably more than offset by the reduction in the number of grid points.

The realization that much greater meshing flexibility is desirable for extending the range of validation of spectral wave models provided one strong stimulus for pursuing the work reported here. However, in the past decade, unstructured mesh spectral wave models have been developed and applied in a number of studies. The semi-Lagrangian model TOMAWAC (Benoit et al., 1996) is probably the first spectral model that employs triangular elements. The advection of wave action in the geographical space is approximated by means of wave ray tracking. The performance of this model has been assessed to examine the capability of representing wave–current interactions on the current eddies. Sørensen et al. (2004) developed the model MIKE21 SW using a cell-centered finite volume method based on unstructured grids. This model utilizes a first order upwind scheme for the approximation of the convective flux in geographical space. This model was verified by comparison with observations for two storm events in the North Sea and in a bay of the German Baltic Sea. Another spectral wave model applied to unstructured meshes, called WWM, is presented in which two strategies have been implemented. Hsu et al. (2005) introduced a Taylor–Galerkin finite element algorithm and later on, Roland et al. (2006) and Zanke et al. (2006) adopted a fluctuation splitting scheme. The model of Hsu et al. (2005) was validated under monsoon and typhoon conditions near Taiwan. In Ferrarin et al. (2008), satisfactory results of the model coupling between a circulation model and the WWM model applied to the Lagoon of Venice have been presented. Recently, Qi et al. (2009) implemented an unstructured mesh spectral wave model within a finite volume framework, called FVCOM-SWAVE. They applied second order upwind schemes in geographical space. This model was then validated on some benchmark test problems and an application near the Gulf of Maine.

This paper presents a new variant of the unstructured-grid procedure for the spectral wind-wave model SWAN. This variant employs the unstructured-mesh analog to the four-direction Gauss–Seidel iteration technique from the structured version of SWAN, requiring few adaptations in the computational kernel. It should be mentioned that this unstructured-grid algorithm is not based on a finite volume or finite element approach. With the route taken here, this model retains the physics and numerics and the code structure of the structured-grid SWAN model, but is able to run on unstructured meshes. Two idealized cases and one realistic case have been conducted for the verification of this unstructured version of SWAN.

2. Model description

The spectral wind-wave model SWAN computes the evolution of wave action density N using the action balance equation (Booij et al., 1999):

$$\frac{\partial N}{\partial t} + \nabla_{\vec{x}} \cdot [(\vec{c}_g + \vec{U})N] + \frac{\partial c_{\theta} N}{\partial \theta} + \frac{\partial c_{\sigma} N}{\partial \sigma} = \frac{S_{\text{tot}}}{\sigma} \quad (1)$$

with

$$S_{\text{tot}} = S_{\text{in}} + S_{\text{wc}} + S_{\text{nl4}} + S_{\text{bot}} + S_{\text{brk}} + S_{\text{nl3}}. \quad (2)$$

The terms on the left-hand side represent, respectively, the change of wave action in time, the propagation of wave action in geographical \vec{x} -space (with \vec{c}_g the wave group velocity vector and \vec{U} the ambient current), depth- and current-induced refraction (with propagation velocity c_{θ} in directional space θ) and the shifting of the radian frequency σ due to variations in mean current and depth (with the

propagation velocity c_{σ}). The right-hand side represents processes that generate, dissipate or redistribute wave energy. In deep water, three source terms are employed. These are the transfer of energy from the wind to the waves, S_{in} , the dissipation of wave energy due to whitecapping, S_{wc} , and the nonlinear transfer of wave energy due to quadruplet (four-wave) interaction, S_{nl4} . In shallow water, dissipation due to bottom friction, S_{bot} , depth-induced breaking, S_{brk} , and nonlinear triad (three-wave) interaction, S_{nl3} , are additionally accounted for. Extensive details on the formulations of these processes can be found in e.g., Ris (1997), Booij et al. (1999) and Holthuijsen (2007).

For the problem to be well-posed, boundary conditions should be provided. The incoming wave components at the seaward boundaries are specified by a two-dimensional spectrum. The closed boundaries, e.g. a coastline and lateral boundaries, are fully absorbing for wave energy fully dissipated and leaving the geographical domain, respectively. The lower and upper boundaries in frequency space are indicated by σ_{min} and σ_{max} , respectively. These boundaries are fully absorbing, although a σ^{-4} diagnostic tail is added above the high-frequency cut-off, which is used to compute nonlinear wave–wave interactions and for computing integral wave parameters. Since the directional space is a closed circular domain, no boundary conditions are needed.

3. Numerical method

It is not the role of this paper to describe the numerical framework of the SWAN model in detail, as it has been extensively discussed in Booij et al. (1999) and Zijlema and Van der Westhuisen (2005). Only those issues dealing with unstructured meshes are presented here. We stressed that these issues will readily be operated with the physics of SWAN.

3.1. Discretization in geographic space

For the sake of clarity of the algorithm description below, we put all the terms but the time derivative and propagation term in the geographical space of Eq. (1) in one term $F(\vec{x}, \sigma, \theta)$:

$$\frac{\partial N}{\partial t} + \nabla_{\vec{x}} \cdot [\vec{c}_{\vec{x}} N] = F \quad (3)$$

with $\vec{c}_{\vec{x}} = \vec{c}_g + \vec{U}$ the geographic velocity vector.

For the time being, we restrict ourselves to triangular meshes. However, other type of meshes can be employed as well, e.g. hybrid grids (consisting of both triangles and quadrilaterals). We consider a triangulation of a geographical domain in which Eq. (3) is solved; see Fig. 1. Every vertex and all the triangles around this vertex are taken into account. Observe that the number of cells around a vertex can be different for all vertices. A vertex-based scheme is used in which the wave action N is stored at the vertices and Eq. (3) is solved in each vertex. We note that the values at boundary vertices are fixed during the computation.

For the time integration, we adopt the first order implicit Euler scheme, as follows

$$\frac{N^n - N^{n-1}}{\Delta t} + \nabla_{\vec{x}} \cdot [\vec{c}_{\vec{x}} N^n] = F^n \quad (4)$$

where Δt is the time step and n is the time step counter. The main property of this approximation is that it does not suffer from the stability restriction imposed by the CFL condition inherent in the explicit methods. The unconditional stability of this scheme makes SWAN suitable for use in shallow water, as an operationally acceptable, i.e. relative large, time step can still be chosen. This does not imply that this time step can be chosen arbitrarily. Yet, the time step is limited by the desired temporal accuracy or by a typical time

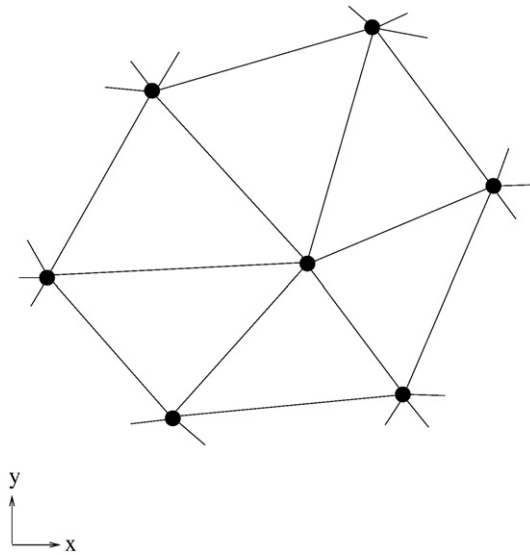


Fig. 1. An example of triangulation.

scale of the phenomena to be simulated. This procedure, however, involves the solution of a large system of equations. A point-to-point multi-directional Gauss–Seidel iteration technique is employed for updating all grid vertices (Zijlema and Van der Westhuysen, 2005). A key feature of this technique is that it is only locally implicit and so, it takes advantage of the newly acquired vertex values during an iteration. In other words, it circumvents the need to build or store large matrices.

We consider the update of a vertex as labeled 1 in Fig. 2. This involves looping over each cell of this vertex. Considering a triangle $\Delta 123$ where the faces towards vertex 1 are given by

$$\vec{e}_{(1)} = \vec{x}_1 - \vec{x}_2, \quad \vec{e}_{(2)} = \vec{x}_1 - \vec{x}_3 \quad (5)$$

with $\vec{x}_i = (x_i, y_i)$ the position vector of vertex i in a Cartesian coordinate system. The action densities at vertices 1, 2 and 3 are denoted by N_1, N_2 and N_3 , respectively. The propagation term of Eq. (3) may be approximated as follows

$$\nabla_{\vec{x}} \cdot [\vec{c}_{\vec{x}} N] \approx c_x N_2^1 e_1^{(1)} + c_x N_3^1 e_1^{(2)} + c_y N_2^1 e_2^{(1)} + c_y N_3^1 e_2^{(2)} \quad (6)$$

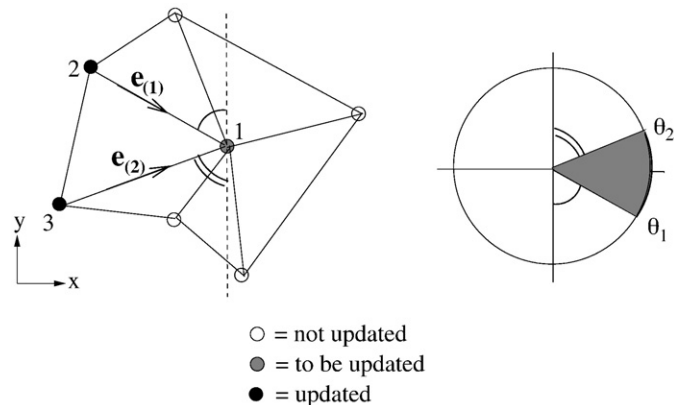


Fig. 2. Update of the wave action at vertex 1 in a triangle $\Delta 123$ and the shaded directional sector in spectral space for which the waves are propagated.

where c_x and c_y are the x - and y -components of the wave propagation vector $\vec{c}_{\vec{x}}$, respectively, and

$$\vec{e}^{(1)} = \frac{1}{D} (e_{(2)}^2, -e_{(2)}^1)^\top, \quad \vec{e}^{(2)} = \frac{1}{D} (-e_{(1)}^2, e_{(1)}^1)^\top, \quad D = e_{(2)}^2 e_{(1)}^1 - e_{(1)}^2 e_{(2)}^1. \quad (7)$$

For the derivation of Eq. (6), see Appendix A. This space discretization is first order accurate and conserves action. Given the action densities N_2^n and N_3^n at vertices 2 and 3 of triangle $\Delta 123$, the wave action in vertex 1 is readily determined according to

$$\left[\frac{1}{\Delta t} + c_{x,1} (e_1^{(1)} + e_1^{(2)}) + c_{y,1} (e_2^{(1)} + e_2^{(2)}) \right] N_1^n = \frac{N_1^{n-1}}{\Delta t} + (c_{x,2} e_1^{(1)} + c_{y,2} e_2^{(1)}) N_2^n + (c_{x,3} e_1^{(2)} + c_{y,3} e_2^{(2)}) N_3^n + F^n. \quad (8)$$

The upwind difference scheme (6) has two main advantages. First, it forces the propagation of wave action to follow the characteristics. Second, it is monotone (i.e. guaranteeing $N > 0$ everywhere; see Section 3.2) and compact (i.e. operating on one triangle only). A disadvantage of this scheme is that it is numerically diffusive, which naturally degrades the accuracy of the model. This numerical diffusion is caused by gradients of wave action across geographic space, e.g. due to refraction by bathymetry or currents. It must be stressed that in the source/sink terms of the action balance equation there is only coupling between the wave components in each grid point separately, not over the grid points. As a consequence, these terms will not tend to enhance numerical diffusion.

The author's main interest is in simulating wind-generated waves and combined swell-sea cases in coastal ocean waters using triangular meshes, and it is particularly with the view to such computations that a simple and compact, but first order, scheme was implemented in the unstructured version of SWAN. Implementation of a higher order upwind scheme, such as SORDUP (Rogers et al., 2002), in the unstructured version of SWAN would have been possible, in principle. This route has not been chosen here, however, for two reasons. First, in view of the complexity of the present numerical strategy and geometry, it is highly desirable to have a robust implementation, while avoiding the algorithmic complexity and computational overhead. Second, a substantial body of experience gathered over the past 10 years on the performance of both lower and higher upwind schemes in SWAN suggests that in many circumstances, the discretization of the propagation terms in geographical space is not a crucial issue. Many nearshore simulations have shown the solution for action density to be on the whole rather insensitive to the accuracy with which geographic propagation terms are approximated. This reflects the tendency for the level of wave action to be dictated by source terms, while the local changes of the energy field across

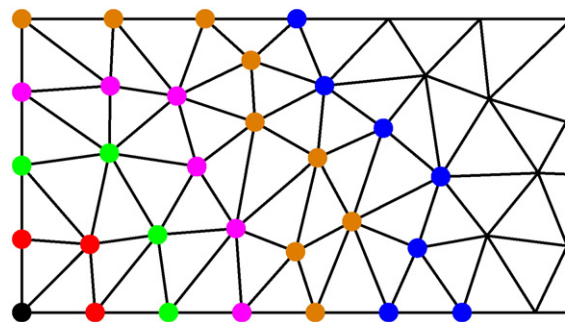


Fig. 3. Ordering of vertices along spherical wave fronts indicated by different color points. The black point in left-bottom corner is chosen as reference point. (For interpretation of the references to color in this figure legend, the reader is referred to the web version of this article.)

geographical space is relatively weak. This is consonant with the established view that a certain amount of numerical diffusion can be safely tolerated in the numerical scheme for geographic propagation, as its impact on wave parameters is negligible (Rogers et al., 2002; WISE Group, 2007). This would appear to suggest, however, that the use of higher order upwind schemes serves no useful purpose. This is probably not so since there might be some cases that are prone to diffusion, where the benefit of such schemes is obvious. One can think of a case of swell propagation over very long distances. While low-diffusive, higher order schemes did permit long-distance swell cases to be validated, the reduced diffusion was found to pose a serious difficulty as the well-known garden sprinkler effect becomes more visible, see e.g. WISE Group (2007).

3.2. Discretization in spectral space

The spectral space is divided into elementary bins with a constant directional resolution $\Delta\theta$ and a constant relative frequency resolution $\Delta\sigma/\sigma$ (resulting in a logarithmic frequency distribution). This spectral

grid resolution is the same in all vertices. The reader is referred to Zijlema and Van der Westhuysen (2005) for further details.

The wave directions between faces $\vec{e}_{(1)}$ and $\vec{e}_{(2)}$ enclose all wave energy propagation in between the corresponding directions θ_1 and θ_2 as indicated as a shaded sector in Fig. 2. This sector is the domain of dependence of Eq. (8) in vertex 1. Since, the wave characteristics lie within this directional sector, this ensures that the CFL number used will properly capture the propagation of wave action towards vertex 1. So, propagation is not subjected to a CFL stability criterion. Also, the coefficients of N_2^s and N_3^s in Eq. (8) remain non-negative implying monotonicity.

Next, the term F^i in Eq. (8) is discretized implicitly in the sector considered. Since, the approximation in the spectral space and the linearization of the source terms are well explained in Zijlema and Van der Westhuysen (2005), we shall not pursue them any further. Eq. (8) constitutes a coupled set of linear, algebraic equations for all spectral bins within the sector considered at vertex 1. Note that the storage requirement of this linear system is low, as only, at most, five matrix coefficients in the whole spectral grid for each geographical

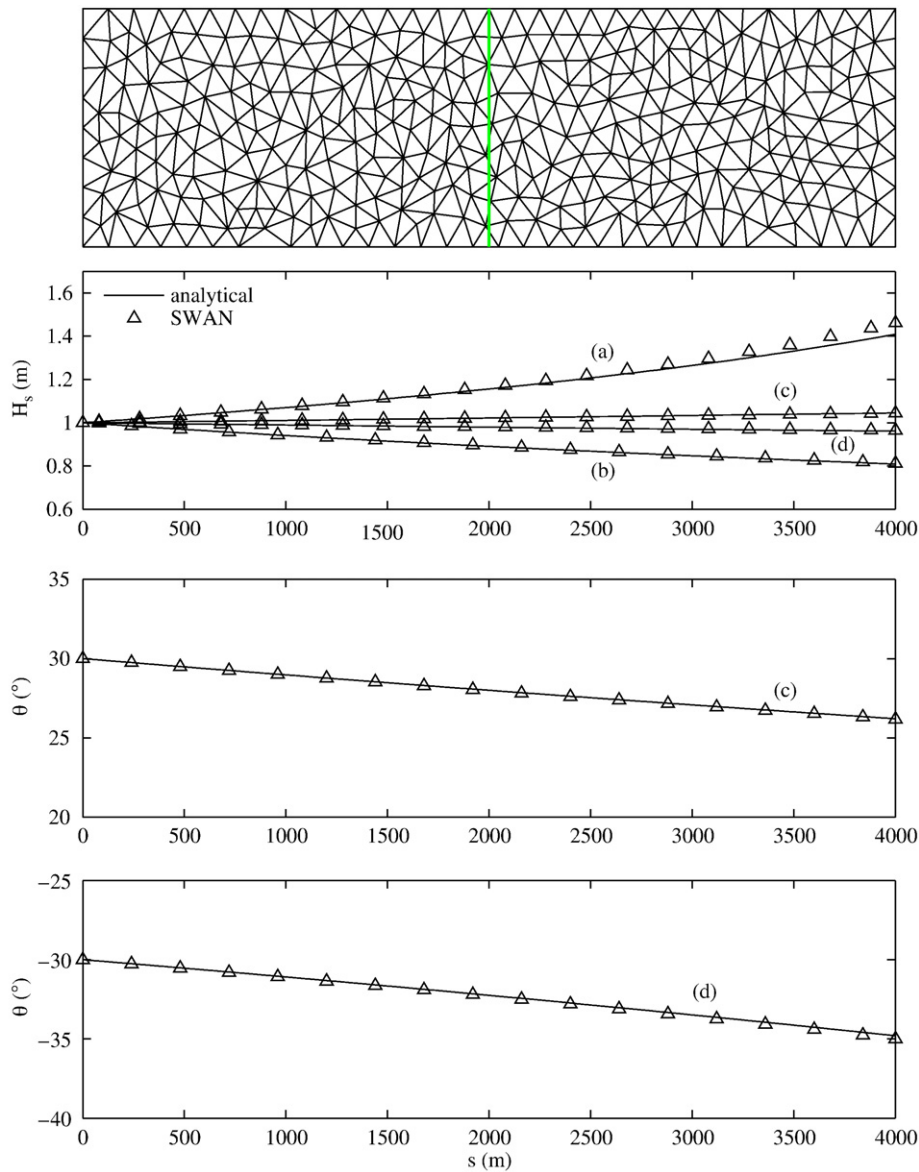


Fig. 4. Current-induced shoaling and refraction for monochromatic, long-crested waves. First panel: unstructured grid with green line as output transect. Second panel: significant wave height along output transect. Third and fourth panel: mean wave direction along output transect. Case (a) an opposing current, case (b) a following current, case (c) a slanting current with incident direction $\theta_i = 30^\circ$ and case (d) a slanting current with incident direction $\theta_i = -30^\circ$.

grid point have to be stored. The solution is found by means of a direct or an iterative solver (Zijlema and Van der Westhuysen, 2005).

The update of vertex 1 is completed when all surrounding cells have been treated. This allows waves to propagate from all directions. Due to refraction and nonlinear interactions, wave energy shifts in the spectral space from one directional sector to another. This is taken into account properly by repeating the whole procedure with converging results.

3.3. The sweeping algorithm

The solution of each vertex must be updated geographically before proceeding to the next one. For example, referring to Fig. 2, the value in vertex 1 is determined by its two upwave vertices 2 and 3 only if they are already updated. For regular grids, the four-sweep scheme based on a four-direction Gauss–Seidel relaxation is employed as outlined in Zijlema and Van der Westhuysen (2005). The grid points are ordered in a natural manner, e.g. left to right and bottom to top during the first sweep, right to left and bottom to top during the second sweep, and so on. Hence, the updated values will be used immediately for updating the next unknown. However, in an unstructured mesh there are no distinct directions. Thus the vertices are ordered by their numbering which for an unstructured grid are quite random. As a consequence, the latest obtained solution will not be necessarily used for updating surrounding vertices.

An ordering is proposed such that the solution of each vertex will tend to ensure that updated values from the surrounding vertices are used as soon as they are available. We introduce a reference point on the boundary where the incoming wave energy is imposed and order all the vertices according to their distances to the reference point in ascending order. The updates along this ordering of vertices can be interpreted as propagation of spherical wave fronts with a center on the upwave boundary through the domain as illustrated in Fig. 3. It is

expected that this specific ordering should result in a faster convergence than a random ordering of vertices.

An algorithm is employed that consists of simply proceeding through a list of vertices that remain to be updated. This list is sorted according to the ascending distances of vertices to the chosen reference point. For a given vertex to be updated using Eq. (8), we first check if its upwave neighbours have already been updated. If this is the case, this vertex is updated and tagged in the list. Otherwise, the considered vertex is placed untagged and the process continues with the next vertex in the list of non-updated vertices. These updates are swept in two cycles. The first cycle involves a forward sweep from the first vertex in the list to the last. The second cycle moves backward from the last to the first. As such, all directions of characteristics can be covered effectively. An iteration is completed when all vertices are updated in both geographic and spectral spaces so that wave energy from all directions has been propagated through geographical space. This numerical process is iterated until an *a priori* convergence condition is satisfied. In the present study, the so-called curvature-based stopping criteria proposed by Zijlema and Van der Westhuysen (2005) will be applied.

4. Verification

For the verification of the performance of the unstructured version of SWAN, a suite of test cases, the so-called ONR Test Bed (Ris et al., 2002), has been conducted. Two academic test cases have been selected in the present paper for the discussion on the verification, where the performance of the geographic propagation scheme applied on unstructured meshes is demonstrated. A third realistic wind-sea case is considered to demonstrate the ability of the model to simulate wind waves entering a complicated bathymetry. These cases are, however, stationary ones as the travel time of the waves through the considered model areas is small compared to the time scale of atmospheric and hydrodynamic conditions.

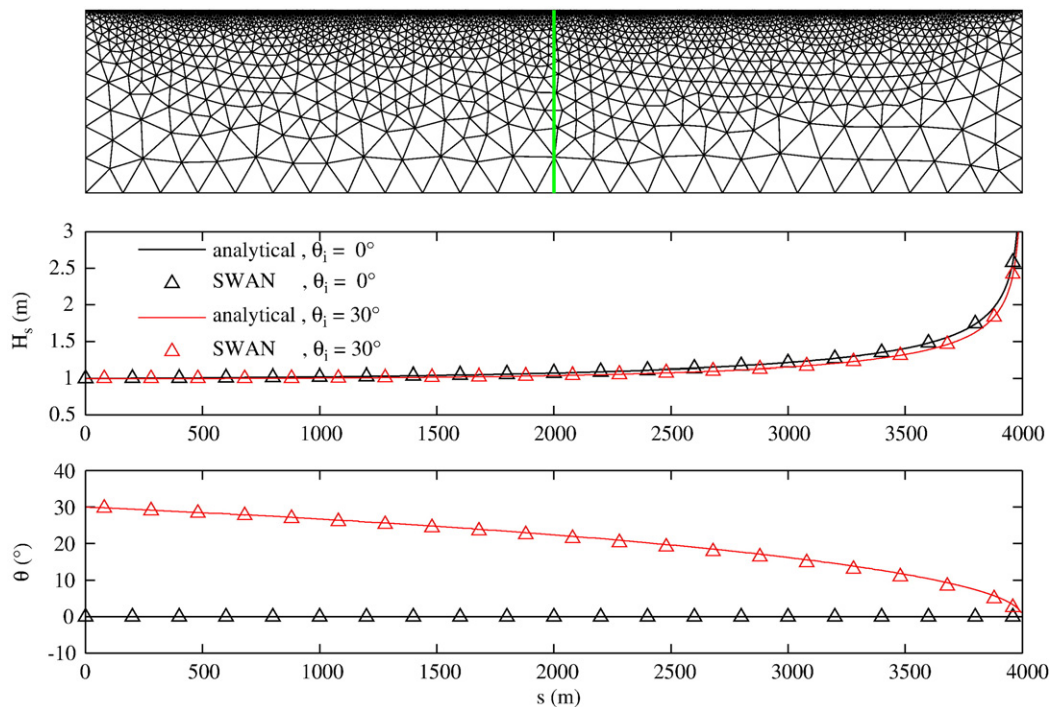


Fig. 5. Depth-induced shoaling and refraction on a plane beach. Top panel: unstructured grid with green line as output transect. Middle panel: significant wave height along output transect. Bottom panel: mean wave direction along output transect. Case with incident direction $\theta_i = 0^\circ$ (black lines, black triangles) and case with incident direction $\theta_i = 30^\circ$ (red lines, red triangles). (For interpretation of the references to color in this figure legend, the reader is referred to the web version of this article.)

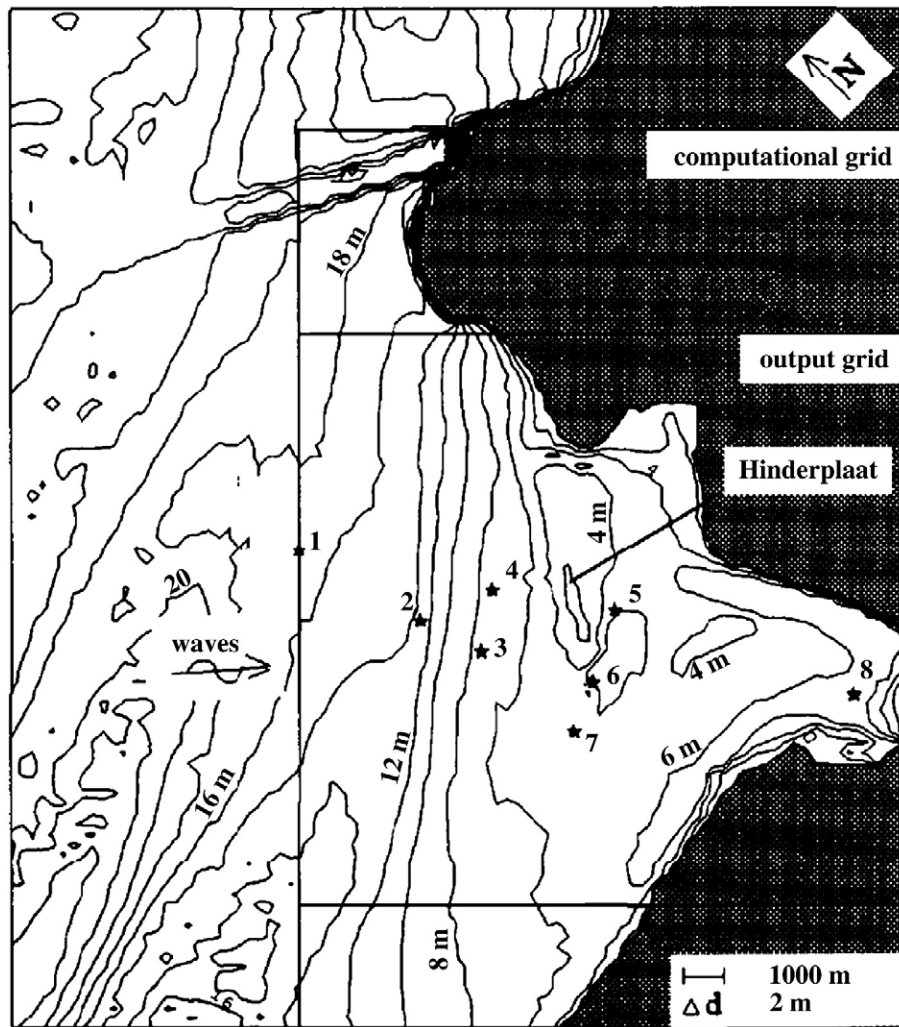


Fig. 6. Bathymetry of the Haringvliet estuary during field campaign of 1982, including the locations of the observation stations 1 to 8 (stars). Depth contours in meters below the Dutch datum NAP (after Ris, 1997).

It ought to be pointed out that the main intention of the present study is to verify unstructured-mesh SWAN in terms of both correctness of coding and numerical accuracy. Therefore, physical issues are not addressed in detail. The predictive performance of SWAN for the cases considered herein, in particular the Haringvliet estuary case (Section 4.3), and generally for other well-documented field cases is examined in other studies, e.g. Ris (1997) and Booij et al. (1999).

4.1. Current-induced shoaling and refraction

We investigate the performance of unstructured-grid SWAN in the presence of an ambient current in deep water. We consider four cases: (a) wave travelling in an opposing current, (b) wave travelling in a following current, (c) wave travelling across a slanting current at an angle of 30° and (d) wave travelling across a slanting current at an angle of -30° . For all four cases, the current velocity increases linearly from 0 to 2 m/s in the down-wave direction. The travel distance of the waves is 4 km. The incident wave is specified by a significant wave height of 1 m and a peak period of 10 s. This wave is monochromatic (modelled with a Gaussian-shaped frequency spectrum with $\sigma_\sigma = 0.01$ Hz) and long-crested (modelled with a $\cos^{500}(\theta)$ directional distribution).

A rectangle domain is considered with a length of 16 km and a width of 4 km. Computations have been performed on an unstruc-

tured mesh with an average size of 400 m. The frequency resolution is equal to $\Delta\sigma = 0.04\sigma$ between 0.05 Hz and 0.25 Hz. The directional resolution is 2° for cases (a) and (b) and 1° for cases (c) and (d). The source terms are not activated. This permits a direct comparison with an analytical solution of the linear wave theory for the total energy (see e.g. Ris, 1997). Comparison is made for significant wave height and mean wave direction. The results are shown in Fig. 4. Clearly, the calculated wave parameters match very well with the analytical solutions, indicating that the geographic propagation scheme, i.e. Eq. (6), is implemented correctly. There is some evidence that the sensitivity of predicted wave parameters to the order of this scheme is negligible in this case, as the employed unstructured mesh is quite coarse and the geographic spatial gradient of wave action is marginal.

4.2. Depth-induced shoaling and refraction

The verification of depth-induced shoaling and refraction on a plane beach is discussed. We consider monochromatic, long-crested waves approaching an infinitely long plane beach with slope 1:200. The maximum water depth is 20 m. When these waves approach the plane slope from another direction, depth-induced refraction occurs. All source terms are set equal to zero so that shoaling dominates. We consider a test with normal incidence waves (shoaling only) and a test with wave direction turning over 30° (shoaling and refraction). In all the computations, the incident significant wave height and the wave peak

period is 1 m and 10 s, respectively. The mesh employed has a maximum size of about 800 m and a minimum size of about 20 m near the shoreline. The directional resolution is 0.5° and the frequency resolution is $\Delta\sigma = 0.04\sigma$ between 0.05 Hz and 0.25 Hz. The results are shown in Fig. 5 with an excellent agreement with the linear theory.

4.3. The Haringvliet estuary

The Haringvliet is a branch of the Rhine estuary in the south-west of the Netherlands. A well-documented field campaign in this area was carried out in 1982 (Andorka Gal, 1995). The bathymetry of the area and the locations of the eight observation stations are shown in Fig. 6. The shallow bay that penetrates into the shoreline is partly protected from the North Sea by a shoal called the “Hinderplaat”. Wave energy dissipates near this shoal. Far behind the shoal, waves are regenerated by the local wind. This case is one of the many field cases of the ONR Testbed (Ris et al., 2002).

The grid for the Haringvliet estuary is generated using the mesh generation package BatTri (Bilgili and Smith, 2003). First, a relatively coarse mesh is created as depicted in Fig. 7. The bathymetry is interpolated onto the grid. The next step is to refine the mesh. In this example, the h -refinement is applied that relates the maximum triangle area to water depth. The final mesh for the present study of

Haringvliet estuary is shown in Fig. 8. This mesh has 4641 vertices and 8866 triangles. Clearly, the size of the triangles is proportional to the depth. The minimum size of the cells is roughly 25 m and is to be found in the Hinderplaat. We compare the model outcomes obtained with this unstructured mesh to that of the simulation using a structured grid. This grid is rectangular and contains 98×88 cells with $\Delta x = 150$ m and $\Delta y = 250$ m (Ris, 1997). The number of active grid points appears to be 5165. Although, this regular grid has approximately the same number of points compared to the unstructured one, it is much coarser in the more shallow parts of the considered area.

A case is selected here of a local storm in the North Sea on October 14, 1982 at 23:00 h local time, which generated waves from north-western direction. The wind speed and the direction were fairly constant, and locally it was 14 m/s from 300° (measured clockwise from the north). There were almost no currents and the water level was 1.7 m above the Dutch datum NAP. The wave energy measured at the offshore station 1 (Fig. 6) was applied as boundary condition at the offshore boundary running along the west side of the model domain. The frequencies ranged from 0.05 to 1.0 Hz and are discretized into 32 bins on a logarithmic scale ($\Delta\sigma/\sigma \approx 0.1$), whereas 36 wave directions are distributed over the full rose at 10° intervals.

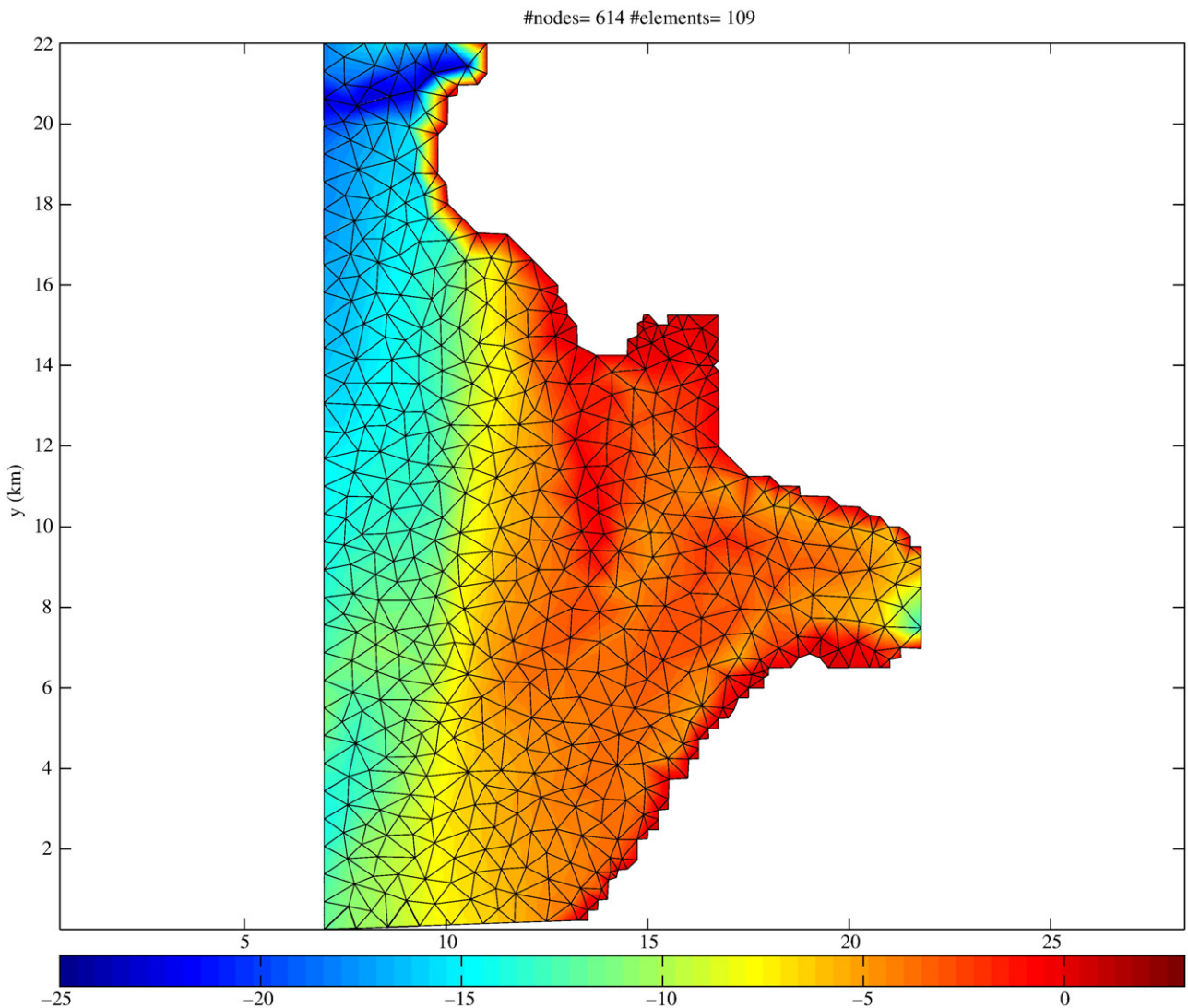


Fig. 7. The initial mesh for Haringvliet estuary, created by BatTri based upon bathymetry (as shown, in meters) and user-supplied parameters.

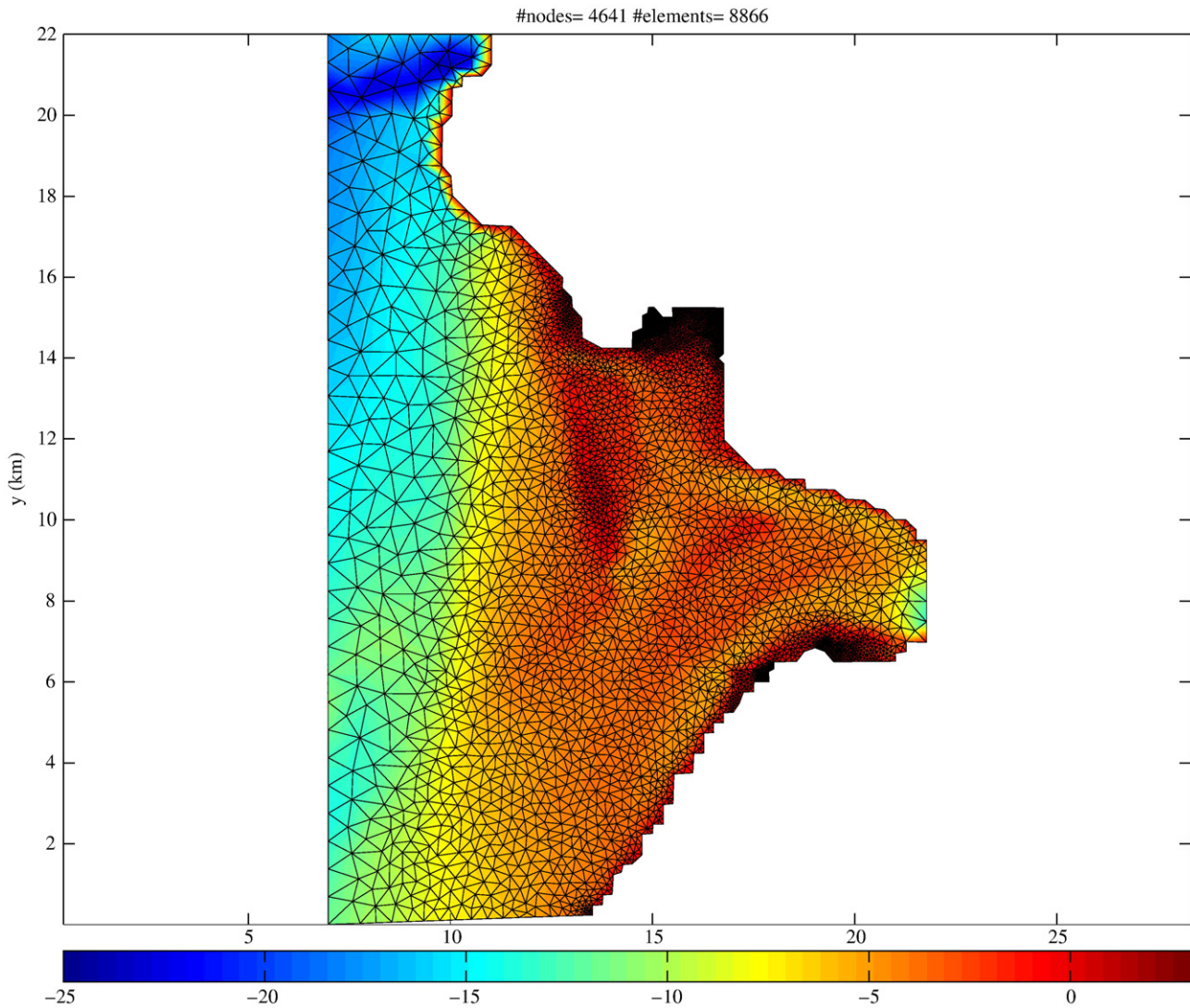


Fig. 8. The final mesh for Haringvliet estuary, as produced by BatTri, refined from the initial mesh based upon h -refinement. Depth in meters.

The simulations were conducted using the default source term settings for deep and shallow water (Booij et al., 1999). Details on the numerics with respect to spectral space can be found in Ris (1997). Here, the regular grid calculation was carried out using the first order upwind scheme in geographic space (BSBT) for consistent comparison.

Considering the intercomparison between grid approaches, the computed frequency spectra at eight locations obtained with unstructured grid are very close to the spectra of the regular one, as can be seen from Fig. 9. Figs. 10, 11 and 12 provide a comparison of plots of significant wave height H_{m0} , mean period T_{m01} and directional spreading σ_θ , respectively, arising from the calculations of unstructured and structured meshes.¹ These figures show good agreement between the computed wave parameters obtained with the employed grids, with relative differences in H_{m0} , T_{m01} and σ_θ being less than 7%, 8% and 10%, respectively. These observed differences are principally rooted in the employed grid resolutions. Finally, the comparison reveals no apparent problems associated with the employed unstructured-grid model.

5. Conclusion

An unstructured-grid algorithm for SWAN has been presented in detail and verified. The algorithm builds on an existing numerical strategy for regular grids by devising an iterative, point-to-point multi-directional Gauss–Seidel based sweeping technique adapted to unstructured meshes. A distinguished key element of the method is an ordering of the vertices according to the way the spherical wave fronts propagate so that advantage is taken of the propagation character of the problem. The examples shown demonstrate the advantage of an unstructured mesh approach and illustrate a key advantage of the sweeping algorithm presented here. Also, the computed results presented in this paper have verified the numerical accuracy and robust nature of the unstructured version of SWAN.

This version stands out in its ability to simulate wave fields over shelf seas, in coastal areas and shallow lakes in an efficient and stable manner, while sufficiently flexible to permit desired local mesh refinements in such areas. Current work focuses on the validation of the unstructured version of SWAN, tightly coupled to a circulation model ADCIRC, for hurricanes in the Gulf of Mexico, southern Louisiana and Mississippi, including Katrina and Rita of 2005 (Dietrich et al., 2009).

¹ For the definitions of the mentioned wave parameters, see Holthuijsen (2007).

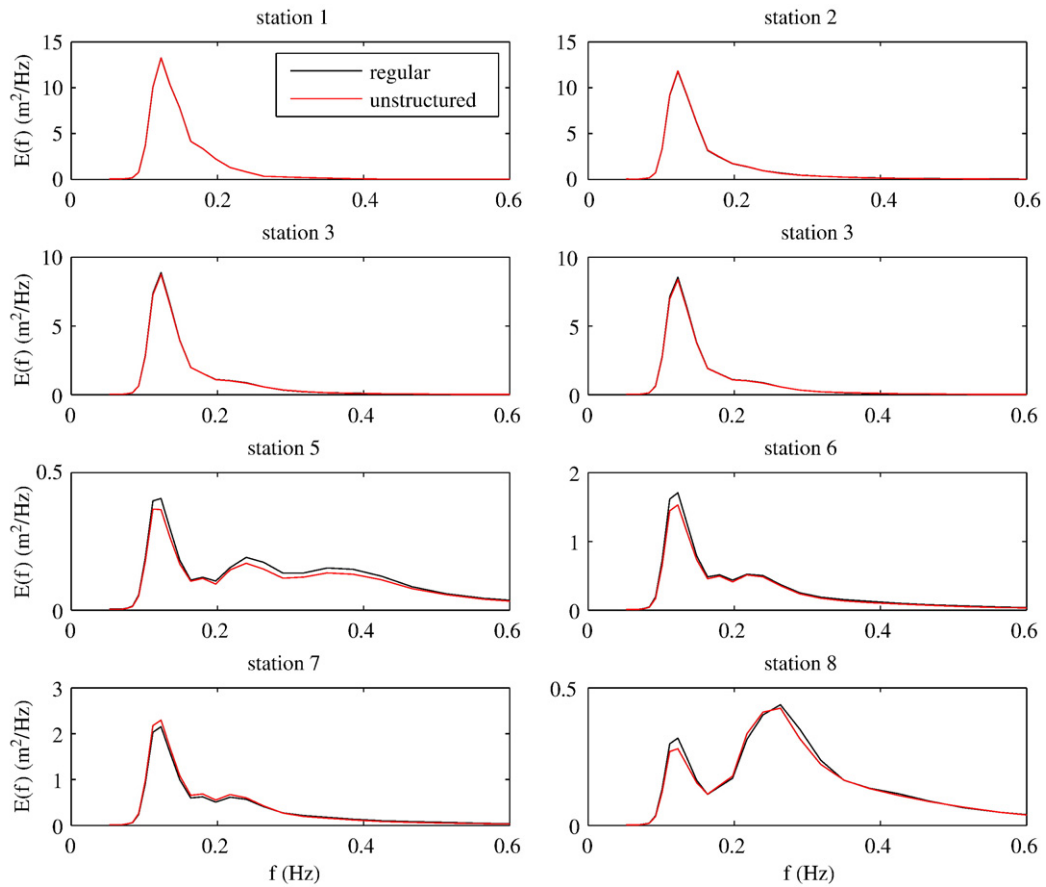


Fig. 9. Computed frequency spectra at eight locations in Haringvliet estuary.

Acknowledgements

This work was partly supported by ONR Grant N00014-06-1-0256. This support is gratefully acknowledged.

Appendix A. Derivation of Eq. (6)

In this appendix we shall derive Eq. (6). To this end, we employ some vector calculus. We consider a triangular cell as depicted in

Fig. 13. In vertex 1, we apply a mapping from a local coordinate system $\vec{\xi} = (\xi, \eta)$ to the Cartesian one $\vec{x} = (x, y)$. Based on this transformation $\vec{x}(\vec{\xi})$, we have the following base vectors that are tangential to the coordinate lines ξ and η , respectively,

$$\vec{e}_{(1)} = \frac{\partial \vec{x}}{\partial \xi}, \quad \vec{e}_{(2)} = \frac{\partial \vec{x}}{\partial \eta}. \tag{A.1}$$

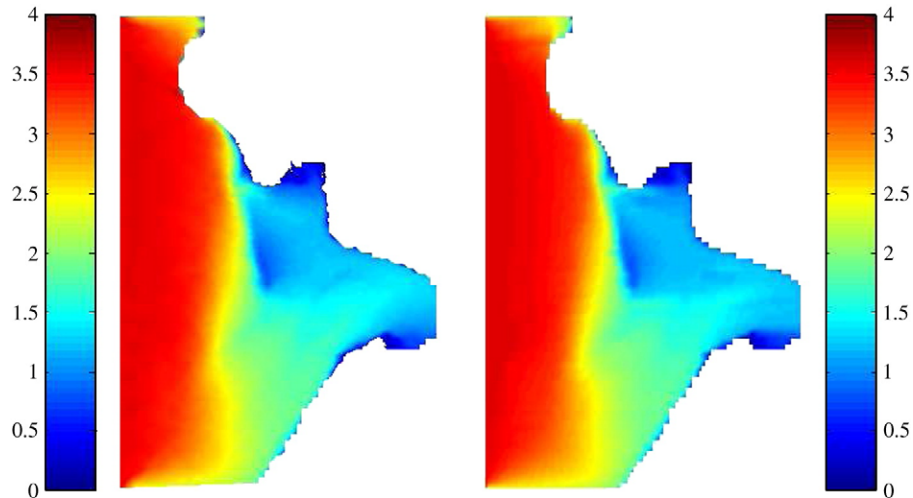


Fig. 10. Significant wave height H_{m0} in meters computed using unstructured grid (left panel) and regular grid (right panel) for the Haringvliet estuary case.

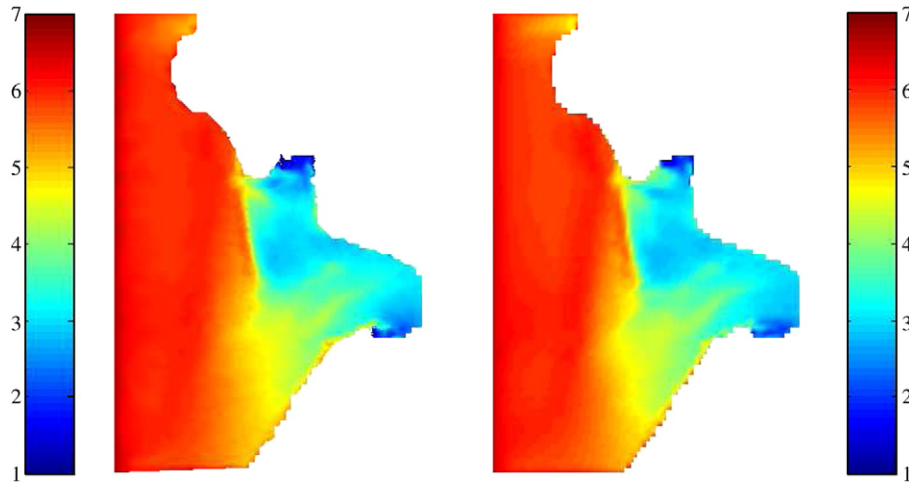


Fig. 11. Mean period T_{m01} in seconds computed using unstructured grid (left panel) and regular grid (right panel) for the Haringvliet estuary case.

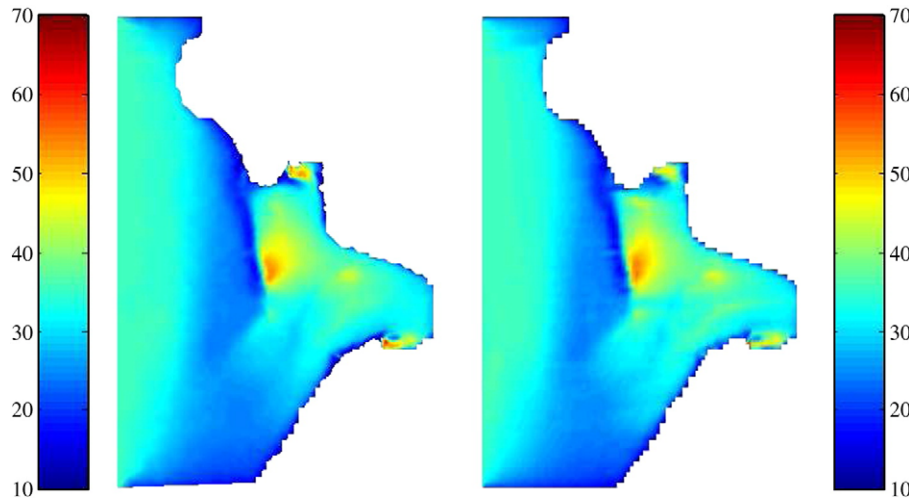


Fig. 12. Directional spreading σ_θ in degrees computed using unstructured grid (left panel) and regular grid (right panel) for the Haringvliet estuary case.

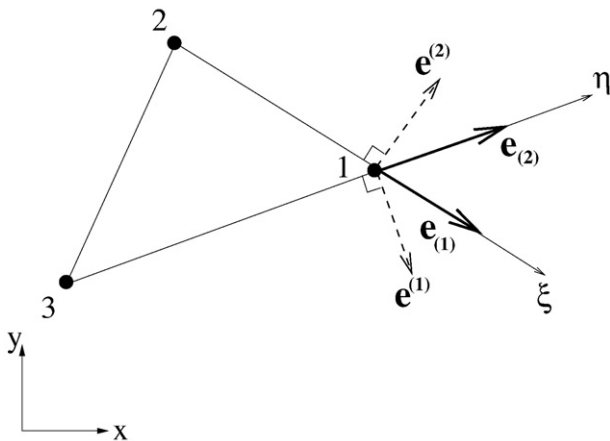


Fig. 13. A triangular cell with geometrical quantities used for discretization in geographical space. Definitions of these quantities are provided in the text.

The vectors

$$\vec{e}^{(1)} = \text{grad}\xi, \quad \vec{e}^{(2)} = \text{grad}\eta \tag{A.2}$$

are normal to the coordinate surface of constant ξ and η , respectively (see Fig. 13). Moreover, they are reciprocal to the base vectors, i.e.

$$\vec{e}^{(\alpha)} \cdot \vec{e}^{(\beta)} = \delta_\alpha^\beta, \quad \alpha, \beta = \{1, 2\}, \tag{A.3}$$

where δ_α^β is the Kronecker delta (which is unity if $\alpha=\beta$, and zero otherwise). Using Cramer's rule, one can find

$$\vec{e}^{(1)} = \frac{1}{D} (e_{(2)}^2, -e_{(1)}^1)^\top, \quad \vec{e}^{(2)} = \frac{1}{D} (-e_{(1)}^2, e_{(1)}^1)^\top, \quad D = e_{(2)}^2 e_{(1)}^1 - e_{(1)}^2 e_{(2)}^1. \tag{A.4}$$

Now we want to approximate the propagation term of Eq. (3). First, we expand this term:

$$\nabla_{\vec{x}} \cdot [\vec{c}_{\vec{x}} N] = \frac{\partial c_x N}{\partial x} + \frac{\partial c_y N}{\partial y}. \tag{A.5}$$

Using the chain rule, we obtain

$$\nabla_{\vec{x}} \cdot [\vec{c}_{\vec{x}} N] = e_1^{(1)} \frac{\partial c_x N}{\partial \xi} + e_1^{(2)} \frac{\partial c_x N}{\partial \eta} + e_2^{(1)} \frac{\partial c_y N}{\partial \xi} + e_2^{(2)} \frac{\partial c_y N}{\partial \eta}. \tag{A.6}$$

Next, we approximate the derivatives in Eq. (A.6). The simplest one is a one-sided first order difference scheme, as follows

$$\frac{\partial c_x N}{\partial \xi} \approx \frac{c_x N|_1 - c_x N|_2}{\Delta \xi}, \quad \frac{\partial c_x N}{\partial \eta} \approx \frac{c_x N|_1 - c_x N|_3}{\Delta \eta}, \quad (\text{A.7})$$

$$\frac{\partial c_y N}{\partial \xi} \approx \frac{c_y N|_1 - c_y N|_2}{\Delta \xi}, \quad \frac{\partial c_y N}{\partial \eta} \approx \frac{c_y N|_1 - c_y N|_3}{\Delta \eta}.$$

Here, we choose the mapping $\bar{x}^*(\bar{\xi}^*)$ such that $\Delta \xi = \Delta \eta = 1$. The derivation is completed by substituting Eq. (A.7) in Eq. (A.6):

$$\nabla_{\bar{x}} \cdot [\bar{c}_{\bar{x}} N] \approx c_x N|_2 e_1^{(1)} + c_x N|_3 e_1^{(2)} + c_y N|_2 e_2^{(1)} + c_y N|_3 e_2^{(2)}. \quad (\text{A.8})$$

Note that the components of the vectors $\bar{e}^{*(1)}$ and $\bar{e}^{*(2)}$ in Eq. (A.8) are given by Eq. (A.4), while the base vectors are calculated according to

$$\bar{e}_{(1)}^* = \bar{x}_1^* - \bar{x}_2^*, \quad \bar{e}_{(2)}^* = \bar{x}_1^* - \bar{x}_3^*. \quad (\text{A.9})$$

References

- Andorka Gal, J.H., 1995. Verification set Haringvliet – October 14, 1982–October 15, 1982. Report RIKZ-95.112x, Ministry of Transport, Public Works and Water Management. The Hague, The Netherlands.
- Benoît, M., Marcos, F., Becq, F., 1996. Development of a third generation shallow-water wave model with unstructured spatial meshing. Proc. 25th Int. Conf. Coastal Engng. ASCE, pp. 465–478.
- Bilgili, A., Smith, K.W., 2003. BatTri: a 2-D finite element grid generator, version 11.11.03. Available from: <http://www.nml.dartmouth.edu/Publications/internal_reports/NML-03-15/>.
- Booij, N., Ris, R.C., Holthuijsen, L.H., 1999. A third-generation wave model for coastal regions. 1. Model description and validation. J. Geophys. Res. 104 (C4), 7649–7666.
- Dietrich, J.C., Zijlema, M., Westerink, J.J., Holthuijsen, L.H., Dawson, C., Luettich, R.A., Jensen, R., Smith, J.M., Stelling, G.S., Stone, G.W., 2009. Modeling hurricane waves and storm surge using integrally-coupled, scalable computations. J. Atmos. Oceanic Techn., in review.
- Ferrarin, C., Umgiesser, G., Cucco, A., Hsu, T.-W., Roland, A., Amos, C.L., 2008. Development and validation of a finite element morphological model for shallow water basins. Coast. Eng. 55, 716–731.
- Holthuijsen, L.H., 2007. Waves in oceanic and coastal waters. Cambridge University Press, Cambridge.
- Hsu, T.-W., Ou, S.-H., Liao, J.-M., 2005. Hindcasting nearshore wind waves using a FEM code for SWAN. Coast. Eng. 52, 177–195.
- Qi, J., Chen, C., Beardsley, R.C., Perrie, W., Cowles, G.W., Lai, Z., 2009. An unstructured-grid finite-volume surface wave model (FVCOM-SWAVE): implementation, validations and applications. Ocean Model. 28, 153–166.
- Ris, R.C., 1997. Spectral modelling of wind waves in coastal areas. Ph.D. thesis, Delft University of Technology, Delft, The Netherlands.
- Ris, R.C., Holthuijsen, L.H., Smith, J.M., Booij, N., Van Dongeren, A.R., 2002. The ONR Test Bed for coastal and oceanic wave models. Proc. 28th Int. Conf. Coastal Engng. ASCE, pp. 380–391.
- Rogers, W.E., Kaihatu, J.M., Petit, H.A.H., Booij, N., Holthuijsen, L.H., 2002. Diffusion reduction in an arbitrary scale third generation wind wave model. Ocean Eng. 29, 1357–1390.
- Roland, A., Zanke, U., Hsu, T.-W., Ou, S.-H., Liao, J.-M., 2006. Spectral wave modelling on unstructured grids with the WWM (Wind Wave Model) II: the deep water case. Third Chinese–German Joint Symposium on Coastal and Ocean Engineering. Tainan, Taiwan. Available from: <<http://www.comc.ncku.edu.tw/joint/joint2006>>.
- Shewchuk, J.R., 1996. Triangle: a two-dimensional quality mesh generator and Delaunay triangulator, version 1.3. Available from: <<http://www-2.cs.cmu.edu/~quake/triangle.html>>.
- Sørensen, O.R., Kofoed-Hansen, H., Rugbjerg, M., Sørensen, L.S., 2004. A third-generation spectral wave model using an unstructured finite volume technique. Proc. 29th Int. Conf. Coastal Engng. ASCE, pp. 894–906.
- Tolman, H.L., 1991. A third-generation model for wind waves on slowly varying, unsteady and inhomogeneous depths and currents. J. Phys. Oceanogr. 21, 782–797.
- WAMDl Group, 1988. The WAM model – a third generation ocean wave prediction model. J. Phys. Oceanogr. 18, 1775–1810.
- WISE Group, 2007. Wave modelling – the state of the art Prog. Oceanogr. 75, 603–674.
- Zanke, U., Roland, A., Hsu, T.-W., Ou, S.-H., Liao, J.-M., 2006. Spectral wave modelling on unstructured grids with the WWM (Wind Wave Model) II: the shallow water case. Third Chinese–German Joint Symposium on Coastal and Ocean Engineering. Tainan, Taiwan. Available from: <<http://www.comc.ncku.edu.tw/joint/joint2006>>.
- Zijlema, M., Van der Westhuysen, A.J., 2005. On convergence behaviour and numerical accuracy in stationary SWAN simulations of nearshore wind wave spectra. Coast. Eng. 52, 237–256.